

Calculating electron current in a tight-binding model of a field-driven molecular wire: Application to xylyl-dithiol

Alexander Tikhonov and Rob D. Coalson^{a)}

Department of Chemistry, University of Pittsburgh, Pittsburgh, Pennsylvania 15260

Yuri Dahnovsky

Department of Physics and Astronomy, and Department of Chemistry, University of Wyoming, Laramie, Wyoming 82071

(Received 11 June 2001; accepted 5 February 2002)

A recently developed Floquet theory-based formalism for computing electron transport through a molecular bridge coupled to two metal electrodes in the presence of a monochromatic ac radiation field is applied to an experimentally relevant system, namely a xylyl-dithiol molecule in contact at either end with gold electrodes. In this treatment, a nondissipative tight-binding model is assumed to describe the conduction of electric current. Net current through the wire is calculated for two configurations of the electrode-wire-electrode system. In one, symmetric, configuration, the electrodes are close ($\sim 2 \text{ \AA}$) and equidistant from the bridge molecule. In the other, asymmetric configuration, one electrode is farther away ($\sim 5 \text{ \AA}$), representing the tip of a scanning tunneling microscope located at this distance from the bridge molecule (the other end being chemisorbed to a gold substrate). For both configurations, electron current is calculated for a range of experimental inputs, including dc bias and the intensity and frequency of the laser. Via absorption/emission of photons, resonant conditions may be achieved under which electron transport is significantly enhanced compared to the unilluminated analog. Calculations show that this can be accomplished with experimentally accessible laser field strengths. © 2002 American Institute of Physics. [DOI: 10.1063/1.1464818]

I. INTRODUCTION

Conduction of electrons through a single molecule connecting two metal electrodes (a molecular wire system) has received significant attention recently.¹⁻³ Experimental studies using both scanning tunneling microscopes (STMs) and mechanical break junctions have been performed.⁴⁻⁷ The configuration consisting of an STM tip in proximity to an adsorbate on a metal surface represents one important type of molecular wire system. Current-voltage ($I-V$) characteristics can be recorded when the tip is positioned above the adsorbate. A related problem of recent interest is conductance through mesoscopic systems composed of semiconductor heterostructures.^{8,9}

Previous theoretical studies suggest that illumination of a molecular electron transfer system by a laser field can alter its conductance properties. Specific motifs that have been studied in this context include: long range metal-metal intramolecular electron transfer complexes,^{10,11} double-barrier semiconductor heterostructures,¹² and systems in which the gap between a metal surface and an STM tip (with no intervening adsorbate) is illuminated.¹³ In a previous article,¹⁴ to be denoted here as Part I, we developed a theory of laser-driven electron transfer through molecular wire systems (ignoring coupling to an external environment). We showed how to use Floquet theory to convert (mathematically) the laser field driven molecular wire system to an effective non-

driven system for which the electron transport rate can be calculated via standard Green-function scattering methods.

In the present paper, we apply the formalism developed in Part I to a realistic molecular wire system consisting of a xylyl-dithiol molecule coupled electronically to two gold electrodes. We have chosen the xylyl-dithiol molecule because it has been extensively studied both experimentally^{6,7,15} and theoretically^{7,16,17} and provides a concrete example on the basis of which to estimate parameters in the system Hamiltonian and to test convergence issues associated with the theoretical analysis.

We consider two different geometries of the molecular wire/electrode system: (1) A symmetric configuration in which the contacts with the gold electrode on either side of the molecule are equivalent. Such a situation approximately obtains in molecular break-junction experiments. Hence we shall term this the "break-junction" configuration. (2) An asymmetric configuration in which the left contact distance is small ($\sim 2 \text{ \AA}$), corresponding to chemisorption of the thiol group on one end of the xylyl-dithiol to a gold electrode, while the other contact distance is considerably larger ($\sim 5 \text{ \AA}$), corresponding to the location of an STM tip. This will be designated as an "STM" configuration. The geometrical differences in these electrode/molecule systems lead to different interactions with the laser field, which in turn results in different induced currents.

The organization of the paper is as follows: In Sec. II, we briefly review the tight-binding model of an ac field-driven molecular wire that was developed in Part I. The key observation there was that the time-dependent Hamiltonian

^{a)} Author to whom correspondence should be addressed; electronic mail: rob@ringo.chem.pitt.edu

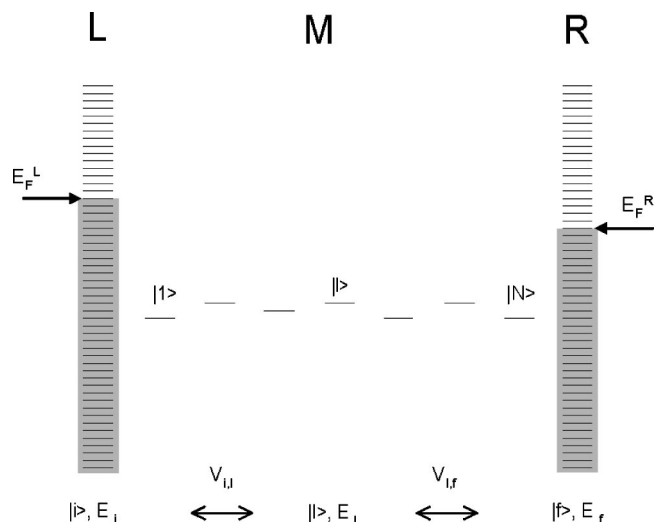


FIG. 1. Energy level and coupling diagram for a molecular wire connected to reservoirs of metallic states. Positions of left and right Fermi levels [for applied voltage $V_{\text{ap}} = (E_F^L - E_F^R)/e_0$] are indicated.

for the field-driven system can be converted, using Floquet theory, into a time-independent Hamiltonian in an augmented state space; and, moreover, this Floquet Hamiltonian has precisely the structure of an “ordinary” (non-field-driven) non-dissipative tight-binding molecular wire system. Hence, standard Green’s functions methods can be directly applied to compute current flow through the laser-driven system. Then, in Sec. III, elementary quantum chemical calculations are performed to determine the parameters which enter into the tight-binding model of xylyl–dithiol coupled to gold electrodes. Next, in Sec. IV, we present some tests on the accuracy of the Floquet/Green’s function analysis of current flow through the field-driven wire. It will be seen that this procedure, carried out to full numerical convergence, provides an exact description of the field-driven system. This motivates our reliance on Floquet/Green’s function analysis for the main results of the paper, which are presented in Sec. V. Here we compute electric current through the xylyl–dithiol wire for both break-junction and STM configurations. A variety of experimental inputs (applied dc voltage, laser amplitude, and frequency) are considered. We highlight conditions that enable significant laser enhancement of electric current through the wires. Finally, our results are summarized in Sec. VI.

II. TIGHT-BINDING MODEL OF AN AC FIELD-DRIVEN MOLECULAR WIRE

A simple one-electron tight-binding model of a molecular wire^{7,18} is depicted schematically Fig. 1. It is comprised of two reservoirs of states, left and right, which represent metal electrodes. Connecting them is a molecular bridge (“wire”). It is useful to briefly summarize the model in the absence of the laser field. This is done in the next subsection (cf. also the corresponding exposition in Part I). The effects of the laser field can then be grafted on (see Sec. II B).

A. Standard molecular wire (no laser field)

The overall system Hamiltonian is defined by the following features. (We follow the notation of Part I throughout.)

The left reservoir states are denoted as $|i\rangle$ and have energy ϵ_i . They are not directly coupled to each other. The same is true of the right reservoir states, which are denoted as $|f\rangle$ and have energy ϵ_f . Left and right reservoir states are not coupled directly to each other. The molecular electronic structure is also represented by a Hückel type Hamiltonian. The N atomic orbitals are denoted $|I\rangle$, with site energies ϵ_I . These states are in general coupled by matrix elements $V_{I,J}$. Finally, coupling between the left reservoir state i and atomic orbital I on the molecular bridge is designated by $V_{i,I}$. Analogously, $V_{f,I}$ designates coupling between the right reservoir state f and bridge atomic orbital I .

The site energy levels just introduced refer to the system in the absence of any external perturbations. In order to get current to flow through the wire, some external field must be applied. In the usual case, a static, dc, field is applied across the metal electrodes using a battery.^{1–8,18–20} This field modifies the electronic Hamiltonian, and in particular, in the one-electron picture adopted here, changes the site energies associated with the tight binding model. We shall term the dc field-dependent site energies as E_i for the left reservoir, etc. If the electric potential associated with the applied electric field is designated as $\phi(\mathbf{r})$, then

$$\begin{aligned} E_i &= \epsilon_i, \\ E_I &= \epsilon_I - e_0 \phi_{I,I}, \\ E_f &= \epsilon_f - e_0 V_{\text{ap}}, \end{aligned} \quad (1)$$

where e_0 is the magnitude of the electronic charge, and $\phi_{I,I} = \langle I | \phi(\mathbf{r}) | I \rangle$. Here the electric potential ϕ is taken, without loss of generality, to be zero throughout the left reservoir (L reservoir) and have the value V_{ap} throughout the right reservoir (R reservoir). The precise functional form of ϕ is complicated by a number of factors,^{7,21} but does not affect the formal development of the one-electron model of molecular wire theory. For simplicity, in the numerical calculations to be presented in this work, we will adopt the simplest reasonable model,²² namely a linear electrostatic potential drop across the junction between the two electrodes (for details, see Sec. V).

Keeping this shift in the “bare” site energies (i.e., the molecular site energies in the absence of applied dc voltage) in mind, the Hamiltonian operator for the system when a voltage is applied across the electrodes reads

$$\begin{aligned} \hat{H} &= \sum_i E_i |i\rangle \langle i| + \hat{H}^M + \sum_f E_f |f\rangle \langle f| \\ &+ \sum_I \sum_i V_{i,I} (|i\rangle \langle I| + |I\rangle \langle i|) \\ &+ \sum_I \sum_f V_{f,I} (|f\rangle \langle I| + |I\rangle \langle f|) \end{aligned} \quad (2)$$

with the bridge Hamiltonian given by

$$\hat{H}^M = \sum_I E_I |I\rangle \langle I| + \sum_{I \neq J} V_{I,J} |I\rangle \langle J|. \quad (3)$$

Associated with the Hamiltonian \hat{H} is a state vector of the form

$$|\psi(t)\rangle = \sum_i c_i(t)|i\rangle + \sum_I c_I(t)|I\rangle + \sum_f c_f(t)|f\rangle. \quad (4)$$

All the basis states are assumed to be orthogonal and unit normalized.²³ The basic dynamical scenario of interest is as follows. The system (electron) is prepared at $t=0$ in a single state i_0 of the L reservoir. We seek to calculate the time evolution of the system for $t>0$, and in particular the probability that the electron makes a transition to state f_0 of the R reservoir, i.e., $|c_{f_0}(t)|^2$. From this the current of electrons moving from the left electrode to the right electrode through the wire can be computed.

By direct solution of the appropriate time-dependent Schrödinger equation, one finds (setting $\hbar=1$ here and throughout)

$$|c_{f_0}(t)|^2 = 2\pi t |\mathbf{v}^L \cdot \mathbf{g}(E_{i_0}) \cdot \mathbf{v}^R|^2 \delta(E_{f_0} - E_{i_0}). \quad (5)$$

Here \mathbf{g} is the Green's function for a modified version of the bridge Hamiltonian. Specifically, it is the $N \times N$ matrix

$$\mathbf{g}(E) = [\mathbf{H}^M - \mathbf{\Sigma}(E) - E]^{-1}, \quad (6)$$

where \mathbf{H}^M is the matrix representing the bridge Hamiltonian [Eq. (3)], and $\mathbf{\Sigma}$ is an E -dependent "self-energy" matrix, which decomposes as

$$\mathbf{\Sigma}(E) = \mathbf{\Sigma}^L(E) + \mathbf{\Sigma}^R(E), \quad (7)$$

with elements

$$\Sigma_{i,I}^L(E) = \sum_I \frac{V_{i,I}V_{I,i}}{E_i - E - i\eta}, \quad (8)$$

and $\eta \rightarrow 0^+$; likewise for $\mathbf{\Sigma}^R(E)$. Furthermore, the elements of the N - d vector \mathbf{v}^L are given by $v_I^L = V_{i_0,I}$, and likewise for \mathbf{v}^R .

From this basic result, it follows that the rate of transitions from an initial state i_0 populated in the L reservoir to isoenergetic states of the R reservoir (provided these are unpopulated in the metal electrode; see below) is

$$r_{i_0} \equiv \frac{1}{t} \sum_{f_0} |c_{f_0}(t)|^2 = 2\mathbf{v}^L \cdot \mathbf{g}(E_{i_0}) \mathbf{\Delta}^R(E_{i_0}) \mathbf{g}^\dagger(E_{i_0}) \cdot \mathbf{v}^L, \quad (9)$$

with $\mathbf{\Delta}^R$ an $N \times N$ "spectral density" matrix given by

$$[\mathbf{\Delta}^R(E)]_{I,I'} = \pi \sum_f V_{f,I} V_{f,I'} \delta(E - E_f). \quad (10)$$

In a standard molecular wire, current is induced by the application of a dc voltage across the two electrodes. This raises the Fermi level of one reservoir relative to the other. For concreteness, let us say that the polarity of the applied voltage is such that $E_F^L > E_F^R$ (cf. Fig. 1). Then, assuming that the temperature is sufficiently low that the $T=0$ limit of the Fermi distribution can be invoked, electrons populating the L reservoir in the energy range $E_F^R < E_{i_0} < E_F^L$ can tunnel isoenergetically into unoccupied states of the R reservoir. The total current I from the left into the right reservoir is then given as the sum of contributions from all incident electronic states in this range,^{7,18}

$$I = \frac{2}{\pi} \int_{E_F^R}^{E_F^L} dE \text{tr}\{\mathbf{\Delta}^L(E) \mathbf{g}(E) \mathbf{\Delta}^R(E) \mathbf{g}^\dagger(E)\} \quad (11)$$

with

$$[\mathbf{\Delta}^L(E)]_{I,I'} = \pi \sum_i V_{i,I} V_{i,I'} \delta(E - E_i). \quad (12)$$

B. Tight-binding model of a laser-driven molecular wire and Floquet mapping to an effective time-independent molecular wire system

Now, suppose that a monochromatic ac electric field of frequency ω and amplitude \mathcal{E}_0 is applied along the axis of the bridge molecule. In the present work, we assume the metal contacts are perfect conductors, so that the electric field inside them is identically zero. We further assume that the electric field imposed by radiation from the light source is not strongly disturbed in the region where the molecular wire is situated, and hence can be considered constant and equal to its free-space value here. With these assumptions, the Hamiltonian of the system is modified to $\hat{H} \rightarrow \hat{H} - e_0 \phi^l \cos(\omega t)$, where ϕ^l is the spatially dependent electric potential established by the light source. ϕ^l is taken to be zero in the left reservoir, to vary linearly across the junction region (where the molecule sits), and to be constant inside the right reservoir. Furthermore, its slope in the junction region is given by $-d\phi^l/dx = \mathcal{E}_0$, with x a the direction perpendicular to the electrodes (we assume the electric field radiated by the light source is polarized in this direction—basically, along the molecular wire).

Thus, in the junction region, the spatial dependence of the radiated electric field takes the form $-e_0 \phi^l = \mu_x \mathcal{E}_0$, where μ_x is the x component of the (negative of the) electric dipole operator: $\mu_x \equiv e_0 x$. We assume further that the electric dipole operator is diagonal in the basis of atomic orbitals ("site orbitals"), due to the small spatial overlap between different orbitals (this overlap falls off exponentially with interorbital separation). Moreover, the diagonal dipole matrix elements are assumed to be given to a good approximation by the position of the site orbital (with all zeroth order states in the L reservoir characterized by the same position, and likewise for the R reservoir). That is, $\langle I | \mu_x | I \rangle = \mu_I = e_0 x_I$, where x_I is the position of the I th atomic site orbital of the bridge molecule. Finally, since the electric potential is assumed to be constant in both reservoirs, we assume that ϕ^l is diagonal in the reservoir states, and has the same value in all L reservoir states, namely $\mu_L = e_0 x_L = 0$ (taking the position of the surface of the left electrode to be at $x=0$). Consequently, in the R reservoir, the diagonal element of ϕ^l implies a value $\mu_R = e_0 x_R$, where x_R is the position of the surface of the metal contact corresponding to the R reservoir.

We note that to the extent that the dipole moment operator is not diagonal in the original site basis $|I\rangle$, one can perform an orthogonal linear transformation which renders it so. This does not compromise the essential structure of the tight-binding Hamiltonian under consideration here. Further details of this procedure are provided in Sec. III C.

The tight-binding Hamiltonian for a general field-driven molecular wire then reads

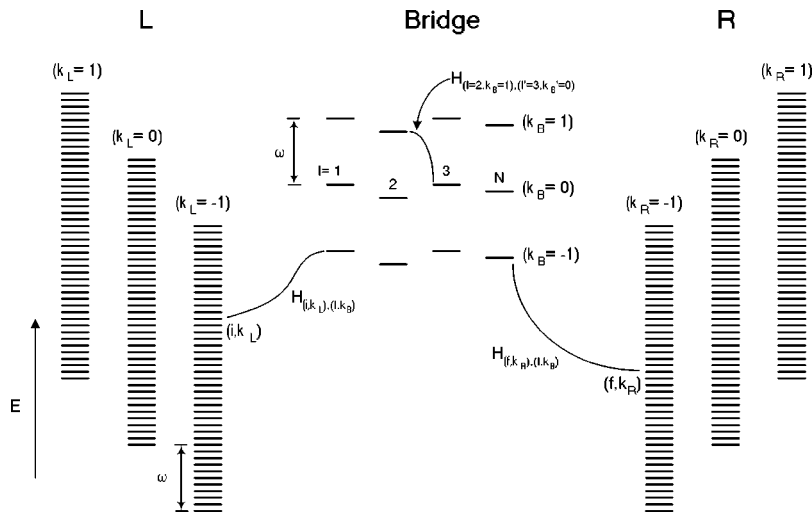


FIG. 2. Floquet state diagram for driven molecular wire system. (Site energies of the physical bridge molecule and metal states are labeled by $k_L=0$, $k_B=0$, $k_R=0$.)

$$\begin{aligned} \hat{H}(t) = & \sum_i (E_i + \mu_L \mathcal{E}_0 \cos(\omega t)) |i\rangle \langle i| \\ & + \hat{H}^M(t) + \sum_f (E_f + \mu_R \mathcal{E}_0 \cos(\omega t)) |f\rangle \langle f| \\ & + \sum_I \sum_i V_{i,I} (|i\rangle \langle I| + |I\rangle \langle i|) \\ & + \sum_f \sum_I V_{f,I} (|f\rangle \langle I| + |I\rangle \langle f|), \end{aligned} \quad (13)$$

with the (driven) bridge Hamiltonian

$$\begin{aligned} \hat{H}^M(t) = & \sum_I (E_I + \mu_I \mathcal{E}_0 \cos(\omega t)) |I\rangle \langle I| \\ & + \sum_{I \neq J} V_{I,J} |I\rangle \langle J|. \end{aligned} \quad (14)$$

As in the nondriven case, associated with this Hamiltonian is a state vector of the form indicated in Eq. (4). Furthermore, the basic dynamical problem is the same as in the zero-field case: calculating the time-evolution of a system (electron) is prepared at $t=0$ in a single state i_0 of the L reservoir.

The field-off limit of this system $\mathcal{E}_0=0$, has been extensively and profitably analyzed using Green's function methods (summarized above).^{7,18} For the field-driven case, it is less obvious how to apply Green's function (GF) techniques, since these require a time-independent Hamiltonian. However, we showed in Paper I that using Floquet theory^{24,25} the periodically time-driven Hamiltonian of interest can be mapped to a (modified and augmented) time-independent form with the same essential structure as in the field-free case. Thus, the GF method can still be applied, and ultimately used to calculate current flow through the wire.

The Floquet Hamiltonian \mathbf{H}^F is associated with an augmented state space. For each state in the physical system, there is a discrete manifold of states in the Floquet system. In other words, in the equivalent Floquet system, there are replicas of the physical states shifted by all integer multiples of the photon quantum. These Floquet states are thus naturally labeled by two indices (α, m) where, again, $\alpha = i, I, f$ de-

scribes the physical state which is replicated and $m = \dots -1, 0, 1 \dots$ labels the replica number. The energy of Floquet state (α, m) [referred to as a "quasienergy," in order to distinguish it from the site energies of the physical states] is

$$E_{\alpha, m} = E_{\alpha} + m\omega. \quad (15)$$

Off-diagonal matrix elements in the Floquet Hamiltonian include: coupling of L reservoir Floquet states to bridge Floquet states

$$H_{(i, k_L), (I, k_B)}^F = V_{i,I} J_{k_L - k_B}(a_{LI}); \quad (16)$$

coupling of Floquet bridge states to other Floquet bridge states

$$H_{(I, k_B), (I', k'_B)}^F = V_{I,I'} J_{k_B - k'_B}(a_{II'}); \quad (17)$$

and, finally, coupling of Floquet bridge states to R reservoir Floquet states

$$H_{(f, k_R), (I, k_B)}^F = V_{f,I} J_{k_R - k_B}(a_{RI}). \quad (18)$$

In these expressions, the a parameters specify appropriate dimensionless field strengths. Specifically,

$$a_{\alpha\beta} = \mathcal{E}_0 (\mu_{\alpha} - \mu_{\beta}) / \omega = -a_{\beta\alpha} \quad (19)$$

with all $\mu_i = \mu_L$, and all $\mu_f = \mu_R$.²⁶

Furthermore, the Floquet coefficients $b_{\alpha, m}$ are related to the physical state amplitudes $b_{\alpha}(t)$ by

$$b_{\alpha}(t) = \sum_{m=-\infty}^{\infty} b_{\alpha, m}(t) e^{im\omega t}; \quad \alpha = i, I, f, \quad (20)$$

where $b_{\alpha}(t)$ is the probability amplitude for physical state α in the interaction picture representation defined by¹⁴ $c_{\alpha}(t) = \exp\{-i\mu_{\alpha}\mathcal{E}_0 \sin(\omega t)/\omega\} b_{\alpha}(t)$.

It is useful to construct a state/coupling diagram for the effective field-off system generated by Floquet analysis, as is done in Fig. 2. This diagram shows clearly that the Floquet Hamiltonian relevant to the driven system has the same generic structure as that of a nondriven molecular wire: both the bridge and the reservoirs are expanded (augmented) in a straightforward manner, and the various couplings coefficients are modified, too.

To represent the physical initial condition $b_{i_0}(0) = 1$ (all other coefficients equal 0), we choose $b_{i_0, k_L=0}(0) = 1$ (all other Floquet coefficients equal 0). From Fig. 2 and the details presented in the preceding paragraphs, it follows immediately that the GF analysis utilized in the case of the non-driven molecular wire can be applied to the Floquet Hamiltonian for the ac field-driven wire.

One important aspect of the connection between the quantum dynamics obtained from the Floquet Hamiltonian and that of the corresponding physical system should be emphasized. For a time-independent Hamiltonian of the type under consideration here, i.e., with the essential structure of Eq. (2), the principle of energy conservation holds: after short time transients, the molecule can only tunnel isoenergetically, i.e., such that the (quasi)energy of the final state in the R reservoir is equal to that of the initially populated Floquet state in the L reservoir. Relating this property to the dynamics of the underlying physical, time-driven system is aided by the following observations.

When one computes (e.g., numerically), dynamics under the time-driven Hamiltonian system prescribed by Eq. (13), it is found that an electron starting from energy level E_{i_0} can end up in the final state $E_{f_0} = E_{i_0} + n\omega$, where n is an integer (positive, negative or zero) corresponding to net absorption of n photons (with negative values of n corresponding to emission).

To connect the behavior of the time-independent Floquet Hamiltonian to that of the underlying time-driven system, one simply has to recognize that different isoenergetic transitions in the Floquet dynamics correspond to photon absorption/emission in the physical system (i.e., have physical final state energies that are shifted from E_{i_0} by integral multiples of the photon quantum). In particular, transitions to the $k_R = 0$ R reservoir replica correspond to net zero photon absorption, transitions to $k_R = 1$ correspond to net one-photon emission, etc. In this way the currents associated with electrons arriving at the various allowed final state energies in the field-driven system can be quantitatively accounted for via Floquet analysis.

Formally, the manifold of Floquet states is infinite. However, the principle of “state mixing,” i.e., that two zeroth order states couple most strongly if they are nearly degenerate, assures that only Floquet replicas which are nearly isoenergetic with E_{i_0} need be retained. In practice we keep the few “most nearly degenerate” Floquet reservoir and bridge replicas and ignore the rest. The number of replicas is expanded until numerical convergence is attained.

C. An “independent channel approximation” to field-driven transport

The mapping of the time-driven Hamiltonian given in Sec. II B to a time-independent Hamiltonian with the same form as the canonical tight-binding molecular wire Hamiltonian leads to a precise way of calculating current flow through a laser-driven molecular wire. As described there, the effective system generated by the Floquet mapping has an augmented bridge comprising $N_b N$ sites, where N is the number of sites in the physical bridge molecule and N_b is the

number of Floquet bridge replicas retained in the calculation. Associated with this augmented bridge is a Floquet bridge Hamiltonian matrix and a Floquet self-energy matrix (the latter being a function of the parameter E). The inverse of the sum of the Floquet bridge Hamiltonian minus the Floquet self-energy minus E times the $N_b N \times N_b N$ unit matrix [directly analogous to Eq. (6) for the field-off molecular wire problem] is the desired $N_b N \times N_b N$ Floquet Green’s function $\mathbf{g}^F(E)$. See Part I¹⁴ for the explicit form of this matrix. Though formally we must take the limit $N_b \rightarrow \infty$ (corresponding to an infinite number of Floquet bridge replicas), in practice convergence can be obtained with a finite and often modest value of N_b , as noted above. Nevertheless, as the calculation gets more complicated, physical insight can become obscured.

Some insight can be restored by considering an approximation introduced in Part I,¹⁴ termed the independent channel approximation (ICA), in which off-diagonal terms coupling different Floquet replicas in the $N_b N$ augmented bridge Hamiltonian and self-energy are neglected. This renders both matrices block diagonal with an $N \times N$ block representing each Floquet replica. Consequently, the GF attains the same block diagonal structure.

In general, the transition probability for an initial state i_0 of the L reservoir to a final state f_0 of the R reservoir, which is nearly on resonance with a net N_p photon emission (corresponding in the Floquet Hamiltonian system to transitions to the R reservoir replica $k_R = N_p$) is

$$|b_{f_0}(t)|^2 \cong 2\pi t \delta(E_{f_0} + N_p \omega - E_{i_0}) |\mathbf{v}^L \cdot \mathbf{g}^F(E_{i_0}) \cdot \mathbf{v}^R|^2, \quad (21)$$

with the $N_b N$ dimensional array \mathbf{v}^L consisting of the coupling elements

$$V_{i_0, J} J_k(a_{IL}); \quad I = 1, 2, \dots, N, \quad k = 1, 2, \dots, N_b.$$

Similarly, \mathbf{v}^R consists of elements $V_{f_0, J} J_{N_p - k}(a_{RI})$.

As noted above, within the ICA the Floquet GF \mathbf{g}^F becomes block diagonal, each block having the dimension N of the physical molecular bridge. Thus, the ICA implies

$$\mathbf{v}^L \cdot \mathbf{g}^F(E_{i_0}) \cdot \mathbf{v}^R \cong \sum_{k_L = -\infty}^{\infty} \mathbf{v}_{k_L}^L \cdot \mathbf{g}^{\text{eff}}(E_{i_0} - k_L \omega) \cdot \mathbf{v}_{N_p - k_L}^R. \quad (22)$$

The matrix \mathbf{g}^{eff} on the right-hand side (r.h.s.) of this expression is an effective molecular Green’s function. It has the dimensions of the physical bridge, i.e., $N \times N$, and also the same generic structure as in the field-off case, namely,

$$\mathbf{g}^{\text{eff}}(E) = (\mathbf{H}_{\text{eff}}^M - \Sigma^{\text{eff}}(E) - E)^{-1}. \quad (23)$$

In this expression, $\mathbf{H}_{\text{eff}}^M$ is an effective molecular bridge Hamiltonian matrix, dimension $N \times N$. Its diagonal elements are the bridge site energies E_I and its off-diagonal elements are renormalized bridge coupling parameters $V_{I, I'} J_0(a_{II'})$. The corresponding effective $N \times N$ effective self-energy matrix $\Sigma^{\text{eff}} = \Sigma^{L, \text{eff}} + \Sigma^{R, \text{eff}}$ is defined as

$$\Sigma_{I, J}^{L, \text{eff}}(E) = \sum_{m = -\infty}^{\infty} J_m(a_{LI}) J_m(a_{LJ}) \Sigma_{I, J}^L(E - m\omega), \quad (24)$$

Σ^L being the left reservoir self energy of the physical (field-off) wire, as prescribed in Eq. (8); and analogously for $\Sigma^{R,\text{eff}}(E)$. Finally, the elements of the N -dimensional vectors $\mathbf{v}_k^{L,R}$ are given by

$$(\mathbf{v}_k^L)_I = V_{i_0,I} J_k(a_{IL}); \quad (\mathbf{v}_k^R)_I = V_{f_0,I} J_k(a_{RI}).$$

The decomposition provided by the ICA enables more rapid numerical evaluation because the size of the matrices which have to be inverted is significantly reduced (particularly for large N_b). However, the primary utility of the channel decomposition is that it provides a way to anticipate the origin of large contributions to the current by associating individual contributions to Eq. (22) with specific electron transfer pathways or “channels.” This interpretation was discussed at length in Part I. Here, we simply reiterate the conditions which validate the approximation. Being predicated on the neglect of off-diagonal matrix elements in the Floquet GF which couple different Floquet bridge replicas, the ICA will be most accurate when electronic coupling matrix elements are small, the laser-field is weak, and/or there is a large energy gap between the quasienergies of different bridge replicas arising from a high photon frequency. In the first two circumstances the elements of the inter-replica coupling blocks go to zero, while in the third there is poor “mixing” between the zeroth order states in separate replicas due to the large gaps between their zeroth order (quasi)energies. The best way to ensure that the ICA is valid is to correct it by coupling several bridge replicas together and verifying that the effects of such coupling are small.

III. PARAMETRIZATION OF THE MODEL

In order for our estimations of laser-induced modifications of electron tunneling through a molecular wire to have at least qualitative value, it is necessary to select a bridge molecule and metal electrodes, and to establish reasonable electronic structure parameters for the one-electron tight-binding model introduced above. For this reason, we consider for concreteness the xylyl dithiol molecule as our “wire,” and gold electrodes (cf. Fig. 3). Xylyl-dithiol is among the simplest systems which have been studied in the context of molecular wires. Its electronic structure has been characterized, at least at the extended Hückel level of electronic structure theory, and it has been shown that this admittedly crude level of treatment produces reasonable agreement with measured I - V curves, in the absence of laser-induced perturbations.⁷ (To our knowledge, a systematic experimental study of laser illumination on molecule wire performance has not yet been carried out.)

In the next subsection, we discuss how to determine the parameters in the bridge molecule tight-binding Hamiltonian. Then we discuss, in turn, how to estimate the electronic coupling between bridge molecule and reservoir, and how to compute the matrix elements of the electric dipole operator (needed to include coupling to a static or an ac electric field).

A. Site-basis representation of the bridge molecule

Following the treatment given in Refs. 7, 16, and 17, we have used extended Hückel (EH) theory to estimate site en-

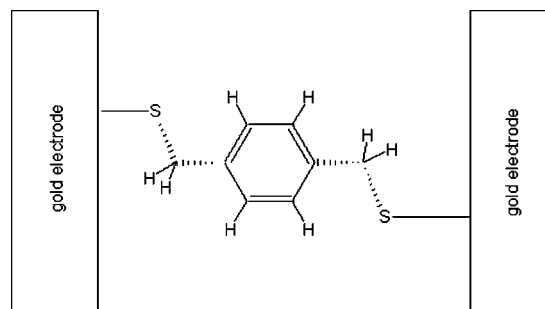


FIG. 3. Chemical structure of xylyl-dithiol molecule connecting two gold electrodes.

ergies and coupling matrix elements in the tight-binding Hamiltonian for the xylyl-dithiol molecule. The site orbitals were chosen to be atomic orbitals (AOs) (details are provided below). The site energy ϵ_I associated with a given AO was taken to be the negative of the ionization potential for removing an electron from that orbital. Specific numerical values were taken from Ref. 27. Intersite coupling elements were determined by invoking the Wolfsberg-Helmholtz approximation²⁸

$$V_{I,J} = \kappa S_{I,J} \frac{\epsilon_I + \epsilon_J}{2}, \quad (25)$$

with $S_{I,J}$ the overlap matrix element for basis atomic orbitals I and J , and $\kappa = 1.75$ an empirically determined scale factor.

The xylyl-dithiol molecule has eight hydrogen atoms, eight carbon atoms and two sulfur atoms. In our calculations we included the $1s$ orbital for the hydrogen, $2s2p$ orbitals for carbon, and $3s3p$ orbitals for sulfur, bringing the total number of basis functions to $N = 48$. The geometric structure of the molecule was obtained by geometry optimization of the isolated molecule using GAUSSIAN 94,²⁹ which was also used to determine the overlap matrix $S_{I,J}$ in the STO-3G basis set.

The EH method is based on rather crude approximations. It was designed to predict the molecular geometry and charge distribution of limited types of molecules, mainly nonpolar hydrocarbons.²⁸ For energy level structure, EH is expected to be only qualitatively correct. For more accurate electron transport calculations one would need a more realistic tight-binding molecular Hamiltonian. A possible step in this direction would be to use a one-electron model with matrix elements deduced from Hartree-Fock (HF) theory.^{30,31} Effects resulting from the connection of the molecule to the gold surface should also be taken into the account: this may alter the equilibrium geometric structure of the xylyl-dithiol molecule. Furthermore, the molecule can acquire additional partial charge which creates an electrostatic potential along the molecule-electrode connection.⁷

To calculate the current through the wire it is crucial to know the position of the Fermi energy level of the metal with respect to the highest occupied molecular orbital-lowest unoccupied molecular orbital (HOMO-LUMO) gap of the bridge molecule. The work function of gold metal is 5.3 eV, hence the Fermi energy is -5.3 eV. Our EH calculations on xylyl-dithiol molecule yield a HOMO energy of -12.3 eV

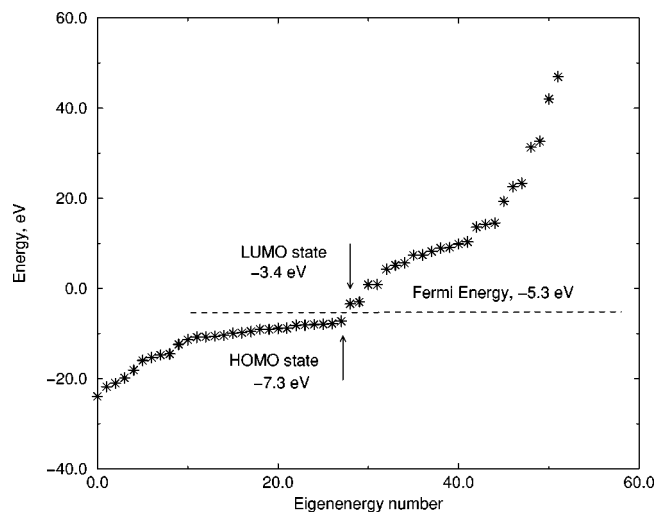


FIG. 4. EH energies for an isolated xylyl-dithiol molecule, after upward shift of EH levels by 5 eV.

and a LUMO energy of -8.5 eV. As noted above, the EH model was not designed to provide accurate absolute orbital energies, so we need to decide how to locate the EH orbital molecular energies relative to the Fermi energy E_F of the gold. Determination of the Fermi energy location should in principle take into account the possibility of charge transfer occurring as a result of attaching the molecule to the electrode. Both experimental and theoretical estimations^{7,17} put the Fermi energy of the electrodes somewhere in the HOMO–LUMO gap, close to the middle of the gap. An *ab initio* HF calculation on isolated xylyl-dithiol using GAUSSIAN 94 with a STO-3G basis set gives a HOMO level energy of about -7 eV, which supports the idea of placing the Fermi energy at the center of the gap.

The calculated energy spectrum of the isolated xylyl-dithiol molecule is presented in Fig. 4. Because the molecule has 54 valence electrons, HOMO and LUMO states correspond to states 27 and 28, as indicated by the arrow. We shifted the EH energy spectrum up by 5 eV, so that the gold Fermi energy lies midway between the HOMO and LUMO states of the molecule. The new HOMO and LUMO energies are then -7.3 and -3.4 eV.

B. Reservoir-bridge coupling matrix elements: Spectral density and self-energy functions

To obtain estimations of the electronic coupling between the electronic states of the metal and those of the molecular wire, we adopt a cluster model for the metal (in our case, gold), and use EH theory (*vide supra*). The xylyl-dithiol molecule binds strongly to the gold surface through a thiol group.¹⁵ The sulfur atom can bind to the gold either over a hollow site on the surface between three gold atoms or directly over a gold atom. Although recent experiments and calculations suggest that binding over the hollow site is more energetically favorable,¹⁷ in the present work we assume the binding takes place over a single gold atom since this is somewhat simpler to analyze. Given the crude electronic structure model used here, this choice should not qualitatively alter our essential conclusions.

We also describe the electronic structure of the reservoirs and the molecule–reservoir coupling using the EH scheme. As noted above, in the model employed here the connection between the molecule and the gold pads occurs through the bond between a single gold(111) atom and the adjacent molecular sulfur atom. For each gold atom we include nine orbitals ($5d6s6p$). The distance between the sulfur atom and the gold atom that it “sits over” is taken to be 1.9 Å (as in Ref. 7). The sulfur–gold overlap matrix was obtained using GAUSSIAN 94 with the gold valence basis functions parameters taken from Ref. 32. Most of the overlap between the sulfur and gold occurs through the s orbital of the sulfur. Thus, we can simplify our calculations by assuming only $V_{i,1} \neq 0$, where 1 corresponds to the $3s$, orbital of the sulfur atom adjacent to the left electrode (L electrode) and, analogously, only $V_{f,N} \neq 0$, where N labels the $3s$ orbital of the sulfur atom adjacent to the right electrode (R electrode).

The gold electrode band structure was obtained from EH calculations for a $5 \times 5 \times 5$ gold(111) cluster using tight-binding parameters from Ref. 33. This was then utilized to calculate the spectral density associated with the coupling of the electrode to the $3s$ orbital of the adjacent sulfur atom. Specifically, we computed

$$\Delta(E) = \pi \sum_p V_p^2 \delta(E - E_p), \quad (26)$$

where the summation was taken over the (extended Hückel level) eigenstates p of the gold atom cluster. We assumed that only the $6s$ orbital of the gold atom over which the sulfur atom is “bound” has a nonzero overlap with the $3s$ orbital of this sulfur atom. The Wolfsberg–Helmholtz prescription 25 was used to calculate the Hamiltonian matrix element connecting these two atomic orbitals, which was then scaled by the appropriate superposition coefficient in each EH eigenstate of the gold cluster to obtain V_p (i.e., the matrix element $V_{i,1}$ in the notation of the previous paragraph).

The resulting spectral density of states is shown in Fig. 5. The “crudeness” of the plot results from numerical fluctuations of the calculations performed on a finite gold cluster. We carried out calculations for three different gold cluster sizes, $3 \times 3 \times 3$, $5 \times 5 \times 5$, and $7 \times 7 \times 7$ —these give similar results for the spectral density (the bigger the size of the cluster the smoother the numerical result). We see from Fig. 5 that the Fermi energy corresponds to states in a broad band with nearly constant $\Delta(E) \approx 4.0$ eV. The largest contribution to the spectral density near the Fermi energy comes from the $6s$ gold band, which is a wide band with relatively constant local density of states at the Fermi energy.

From $\Delta(E)$ we can obtain the self-energy $\Sigma(E)$ as^{7,18}

$$\Sigma(E) = \frac{P}{\pi} \int_{-\infty}^{+\infty} \frac{\Delta(E') dE'}{E' - E} + i\Delta(E). \quad (27)$$

Numerical calculation of the principal value integral 27 based on the spectral density depicted in Fig. 5 gives the real

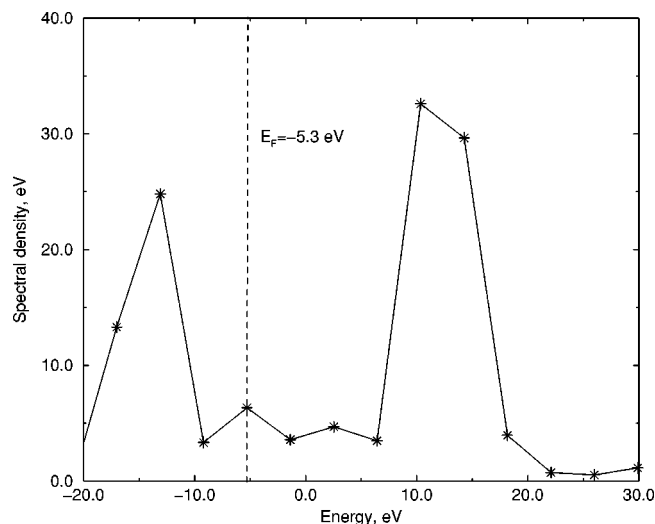


FIG. 5. Spectral density of states for the model where sulfur binds to a single gold atom on the surface of a $5 \times 5 \times 5$ gold(111) cluster. The Fermi energy is located in a region with almost constant spectral density of states comprised mainly of gold s -band states.

part of the self energy to be almost zero within an interval of several eV around the Fermi level. Thus, within this energy regime we can approximate

$$\Sigma(E) \cong 0.0 + 4.0i. \quad (28)$$

We have just described how we calculated the density of states $\Delta_{i,1}$, and corresponding self energy $\Sigma_{i,1}$, where 1 represents the $3s$ orbital of a sulfur atom which is chemisorbed at a distance of 1.9 \AA from the L electrode. If the sulfur atom on the r.h.s. of the molecule is chemisorbed to the R electrode, the same density of states is used for $\Delta_{f,N}$ and the same self energy function for $\Sigma_{f,N}$. For the STM configuration, where the right electrode is 5 \AA from the right sulfur atom, we estimate the relevant spectral density of states using the following empirically established property. In simple models of vacuum STM tunneling,³⁴ the current decreases by about 1 order of magnitude when the tip-surface distance changes by 1 \AA . Hence we multiply the spectral density of states obtained above for the chemisorbed sulfur atom by an appropriate coefficient of proportionality, reflecting the change in separation between the atom and the R electrode.

C. Basis transformation to obtain a diagonal dipole operator

As discussed above, our model assumes a constant dc electric field in the junction region, as well as an ac field of constant magnitude (at any given instant of time) in this region. Thus, the electric dipole operator plays a critical role in our dynamical theory. In particular, if the relevant (static and ac) external electric fields are polarized perpendicular to the metal electrodes (in the x direction), we need to evaluate $\mu_x = e_0 x$, the (negative of the) x component of the dipole operator. It was tacitly assumed in constructing the relevant tight-binding Hamiltonian (see above) that μ_x is diagonal in the molecular site basis. This turns out to be roughly, but not precisely true for the AO site basis introduced above. Thus, it is useful to perform a linear transformation of the site orbit-

als to a set of basis states which are strictly diagonal with respect to the μ_x operator. Details are given next.

The dipole matrix, represented in a localized atomic site basis, was obtained as output from the Gaussian program. The origin of the coordinate system was chosen at the left electrode, hence the dipole moment is zero at the left electrode and increases toward the right electrode. Our Floquet analysis of the system Schrödinger equation assumes¹⁴ that the field-wire coupling occurs only through the diagonal terms in the Hamiltonian. Thus we wish to construct a new orthogonal basis of bridge states in which the bridge dipole matrix is diagonal. We accomplish this through two successive basis transformations. First, from the original nonorthogonal site basis $|\chi_j\rangle$, $j=1..N$ we construct an orthonormal basis ϕ_j , $j=1..N$ via the transformation $\phi_j = \sum_{k=1}^N S_{jk}^{-1/2} |\chi_k\rangle$, where S is the overlap matrix in the χ (site) basis. Next we express the x component of the electric dipole operator in the orthonormal ϕ basis (using the known matrix elements of μ_x in the $|\chi_j\rangle$ basis). Diagonalization of this matrix determines another orthonormal basis, say $|\psi_j\rangle$, $j=1..N$ in which the operator μ_x is diagonal. Finally, the Hamiltonian operator can be expressed in terms of the ψ basis. Inspecting the Hamiltonian matrix elements coupling the wire and electrodes in this basis, we find that the main contributions to the left electrode-bridge coupling occur through two wire basis functions, and two other wire basis functions interact with the right electrode. Thus, for simplicity, in our electric current calculations we set all other small coupling matrix elements to zero.

Note that since there is more than one bridge basis state that couples to the reservoirs, the spectral density and self energy matrices introduced in Sec. II A have more than one nonzero element. However, we assume here that only the $3s$ orbital of the sulfur atom couples electronically to electronic states of the gold electrode. This implies that if we use as bridge basis states the ψ states described in the preceding paragraph, then all nonzero spectral density matrix elements will be proportional to $\Delta(E)$ computed in Sec. III B; likewise, all nonzero self-energy matrix elements will be proportional to $\Sigma(E)$ (again, cf. Sec. III B). The relevant proportionality constants are obtained from the coefficients utilized to expand the ψ basis functions in terms of the original AO (χ) site basis orbitals.

IV. TESTS OF THE FLOQUET MAPPING PROCEDURE

In this section we illustrate the accuracy of the Floquet method developed in Part I to study the quantum dynamics of a field-driven molecular wire, moving beyond the simplistic model studied in Part I, and focusing instead on a realistic (or at least defensible) set of bridge states and interstate couplings. We consider for this purpose the STM configuration, in which the left end of the xylyl-dithiol molecule is located 1.9 \AA from the left electrode, while the right end of the xylyl-dithiol molecule is significantly farther, specifically 5 \AA , from the right electrode.

We solved the time-driven Schrödinger equation corresponding to the Hamiltonian given in Eq. (13) by direct numerical integration of the appropriate set of linear ordinary

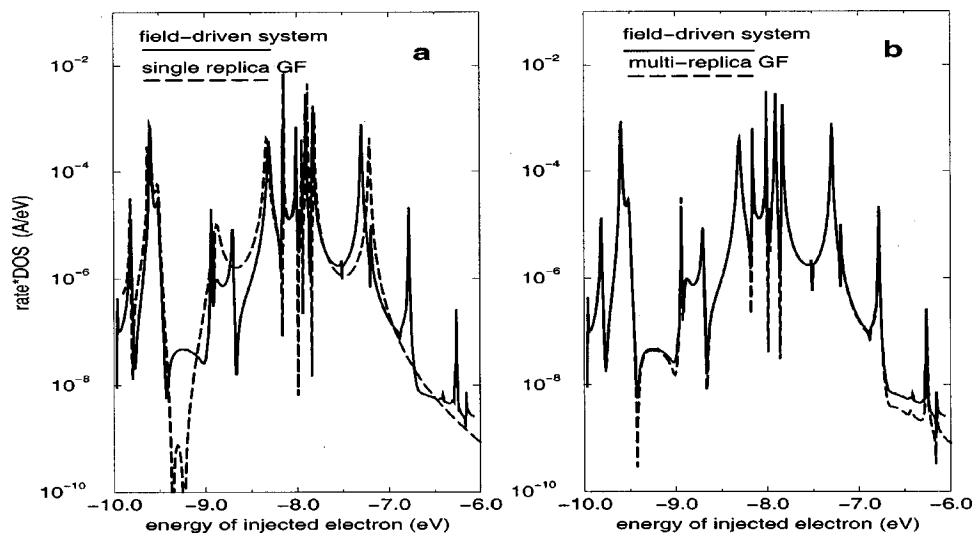


FIG. 6. Tunneling rate dependence on initial energy of the electron in the L electrode. The solid line in both panels shows the result obtained by direct integration of the time-dependent Schrödinger equation for the laser-driven system. In (a) the dashed line shows the result of a restricted Floquet Green's function that retains only one (resonant) replica. See text for details. In (b) the dashed line shows a Floquet Green's function calculation including six bridge and nine L and R reservoir Floquet replicas. Note the good agreement with the result obtained by direct numerical integration of the time-dependent Schrödinger equation in this case. Relevant field parameters are: $\omega=3.8$ eV, $\mathcal{E}_0=2\times 10^7$ V/cm, and $V_{\text{ap}}=0$ in both panels.

differential equations. Starting with population in a single state i_0 of the L reservoir, we calculated the total probability to be in a particular energetic region of the R reservoir (based on energy conservation modulo photon absorption/emission). After short-time transients,¹⁴ a linear growth of the final-state probability was observed, thus defining a transition rate [cf. Eq. (9)]. We then sought to verify via numerical comparison that the Floquet GF method outlined in Sec. II reproduces these rates reliably.

[In practice, direct integration of the time-driven system was done by representing the left and right electronic reservoirs using a finite set of states, evenly spaced in energy, and coupled to the bridge via matrix elements $V_{i,1}$ and $V_{f,N}$ selected in accordance with the spectral densities specified in the previous section. Convergence was obtained by increasing the number of discrete states in the reservoirs, while maintaining the desired (finite) spectral density by reducing the magnitude of the individual reservoir-bridge coupling elements accordingly.]

For a laser frequency of $\omega=3.8$ eV and a laser field strength of $\mathcal{E}_0=2\times 10^7$ V/cm (with no applied static voltage, i.e., $V_{\text{ap}}=0$), we show via the solid line in Fig. 6 the rate of transitions from a range of initially populated states below the Fermi energy ($E_F=-5.3$ eV) of the L reservoir to all final states in the R reservoir above the Fermi level (i.e., transitions to final states with energies less than E_F are blocked). These rates are scaled by the density of electronic states of the L reservoir at the Fermi energy, in order to obtain a finite result in the limit of a dense set of reservoir states. The shape of this "spectrum" reflects the complicated molecular orbital structure of the xylyl-dithiol bridge molecule.

The dashed line in Fig. 6(a) shows a minimum basis attempt to extract the behavior of the time-driven system via Floquet analysis. Specifically, only the replicas $k_L=0$, $k_B=0$, and $k_R=-1$ are retained in the calculation. This corre-

sponds to the following pathway for the incident electron: direct tunneling (without photon absorption/emission) from the L reservoir to the bridge, tunneling across the bridge (without photon absorption/emission), then one-photon absorption to a final state of the R reservoir. It can be seen that this single channel accounts for much of the detail in the exact spectrum, but misses some significant features (resonances). To correct for this shortcoming, we performed a larger basis Floquet GF computation: six bridge replicas (specifically, replicas $-3 \dots 2$) and nine L and R reservoir replicas (specifically, replicas $-4 \dots 4$) were employed. The result is shown via the dashed line in Fig. 6(b). It reproduces the result of direct time-integration of the field-driven Schrödinger equation in all essential details. Thus, we see that the Floquet GF method gives a practical way to obtain rates of electron transmission through a field-driven molecular wire coupled to two metal electrodes, provided proper care is taken to ensure convergence by including a sufficient number of Floquet replicas in the calculation. Consequently, in the numerical computations presented below, we use the GF method, since it is considerably faster than direct integration of the full set of ordinary differential equations required for "brute force" time evolution of the laser-driven system.

The minimum basis calculation just described is tantamount to a skeletal approximation to the ICA formula Eq. (22) in which only one term in the sum over amplitudes is retained. We show in Fig. 7(a) how this single term approximation compares to the full ICA result (using the same field parameters employed in Fig. 6). There is no substantial difference between the full ICA result and the single replica approximation to it in the incident electron energy regime considered in Fig. 6. Failures of the ICA and the single replica approximation in this regime are thus due to inter-(bridge) replica coupling (representing photon absorption/emission on the bridge). In Fig. 7 we have extended the

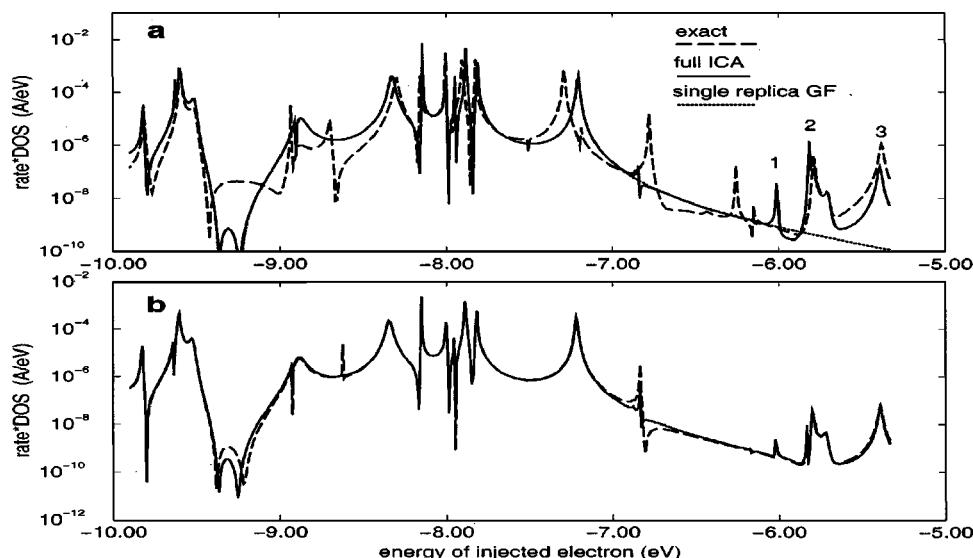


FIG. 7. (a) The exact transition rate as a function of initial electron energy, calculated via the Floquet Green's function method (dashed line) vs the corresponding ICA result (solid line) for the system considered in Fig. 6. For comparison, the "single channel" result shown in Fig. 6(a) is also indicated via the dotted line. (b) The exact (dashed line) vs ICA (solid line) results for the same system when the dimensionless field strength parameters $a_{l,l'}$ inside the bridge are reduced by a factor of 10.

regime of incident energies above -6.0 eV. We see that the full ICA captures the additional peaks in this regime rather well. The origin of these peaks can be traced to other terms in the full ICA sum. In particular, the peaks marked 1 and 2 arise from the $k_B=1$ term and peak 3 arises from the $k_B=-2$ term (in each case we sum over all R reservoir replicas k_R which correspond to final states of the physical R reservoir lying above the Fermi level). As a check on our analysis, we show in Fig. 7(b) a comparison between a converged multireplica Floquet GF calculation versus the corresponding ICA prediction for the case where all the $a_{l,l'}$ parameters are reduced by a factor of 10. Setting these parameters to zero would imply complete suppression of interreplica coupling in the Floquet Hamiltonian, thus improving the accuracy of the ICA. We see that the trend is in the right direction—agreement between ICA and converged Floquet tunnel rate spectra is much better in panel (b) than in panel (a).

Note that none of the transitions indicated in Figs. 6 and 7 would take place in the absence of the laser field, since they correspond to initial states of the L reservoir below the Fermi level. By absorption of photons, electrons initially in these states can "get above" the Fermi energy and access an unoccupied state of the R reservoir.

In fact, it is possible to employ a perturbative expansion for the Floquet GF to systematically correct for the deficiencies of the ICA and to provide insight into the specific intrabridge photon absorption/emission events that contribute to the tunneling rate under various conditions. As noted above, the ICA corresponds to neglect of matrix elements in the inverse of \mathbf{g}^F that connect different Floquet bridge replicas, thus resulting in a block diagonal Floquet bridge Hamiltonian matrix, a block diagonal Floquet self-energy matrix, and hence a block diagonal approximation to \mathbf{g}^F . Treating the neglected matrix elements as the perturbation, a standard GF perturbation expansion can be invoked.³⁵ The first correction to the ICA provides the contribution of all processes that involve one-photon absorption/emission between bridge states, etc. In a subsequent paper³⁶ we will present full details of this expansion and demonstrate that it can correct the

ICA into an essentially exact calculation, except at extremely high laser intensities, where the perturbation expansion diverges.

V. CURRENT THROUGH AN AC DRIVEN MOLECULAR WIRE

Here we present numerical calculations of the electrical current through an ac field-driven xylyl-dithiol molecular wire for a variety of externally tunable parameters. Having shown in Sec. IV that the Floquet GF method enables us to accurately compute the quantum dynamics of the field-driven system, we use it to deduce the current through the wire in all calculations to be presented in the remainder of this paper. (Care was taken to ensure that enough replicas were included in the numerical calculation to obtain converged results for the output current.)

In Sec. V A, we show the predicted current for fixed laser field strength and frequency as a function of applied dc voltage for the (symmetric) break-junction configuration. In Sec. V B, we present analogous calculations for the (asymmetric) STM configuration. Then, in Sec. V C, we investigate in more detail how weak the laser field can be and still produce a significant enhancement of the electron current.

A. Break-junction (symmetric) configuration

Here we consider a symmetric ("break-junction") system, corresponding to chemisorption (covalent bonding) of the xylyl-dithiol molecule at both ends to gold electrodes. For concreteness we take the electrode molecule distance to be 1.9 Å. Also for concreteness, we choose a laser frequency of 1.9 eV, which corresponds to one-half the HOMO-LUMO energy gap. Furthermore, we fix the laser field amplitude at the value $\mathcal{E}_0 = 2 \times 10^7$ V/cm.

In Fig. 8 we show the forward (left to right) and backward (right to left) currents as a function of applied dc bias.³⁷ Their difference (forward minus backward) gives the net left to right current through the wire. [Because a logarithmic scale is used in the graph, vanishing of net current is indicated by the sharp dip (towards $-\infty$) at zero bias. Note also

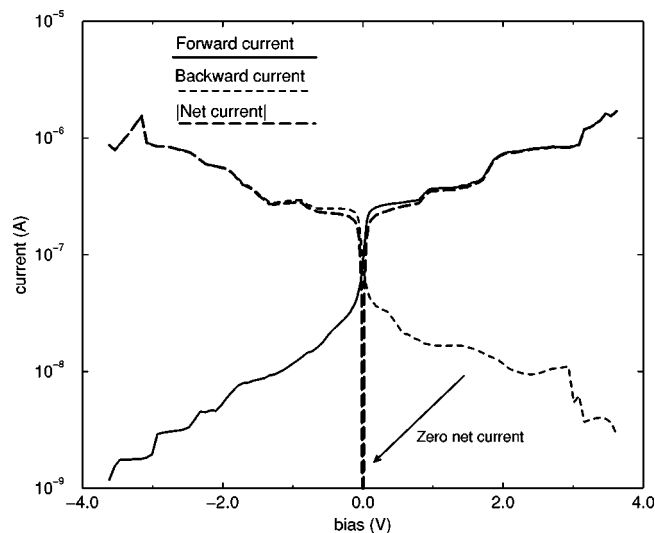


FIG. 8. Laser-assisted current (in amperes) through a xylyl-dithiol wire in the break-junction OTTS (symmetric) configuration. As a function of applied dc voltage (in volts), forward (left to right) current is shown via the solid line, backward (right to left) current via the short-dashed line, and the absolute value of the net current is shown via the long-dashed line. The following field parameters apply: $\omega = 1.9$ eV and laser field strength $\mathcal{E}_0 = 2 \times 10^7$ V/cm.

that the absolute value of the net current is plotted. Current flows in the direction of the applied bias, that is left to right for positive bias and right to left for negative bias.] Notice that due to the geometrical symmetry of the break-junction configuration, the roles of forward and backward currents should simply be switched when the dc voltage polarity is reversed. Some artificial “symmetry breaking” is apparent in these figures, due to slight asymmetry in the numerical placement of the xylyl-dithiol atoms with respect to the metal electrodes. However, this asymmetry is minor, particularly as regards the net, experimentally observable current.

In contrast to the field-off case, where for small bias only electrons near the Fermi energy participate in the tunneling process, in the field-on case, electrons outside the energy regime bracketed by the Fermi levels of the L and R reservoirs participate as well (assisted by photon absorption/emission). Even for zero dc bias, many electrons in the metal reservoirs having energy well below the Fermi level contribute to forward and backward currents.

It is interesting to remark here that the vanishing of the net current at zero bias is due in the field-on case to perfect cancellation (for a symmetric electrode-wire-electrode configuration) of forward and backward currents. In Fig. 9, we again plot the net field-on current, and compare this to the current obtained when the laser field is turned off, all other system characteristics being unchanged. Two points about the magnitude of the current drawn through the wire are relevant. First, for the laser-off system with a modest applied voltage of ~ 1 V, the current is $\sim 10^{-9}$ A, a value which is in order of magnitude agreement with experimental measurements on break-junction systems.⁶ Furthermore, it is clear that *large* enhancement of current flow is obtained over a wide range of dc voltages when a laser field of the amplitude and frequency noted above is applied.

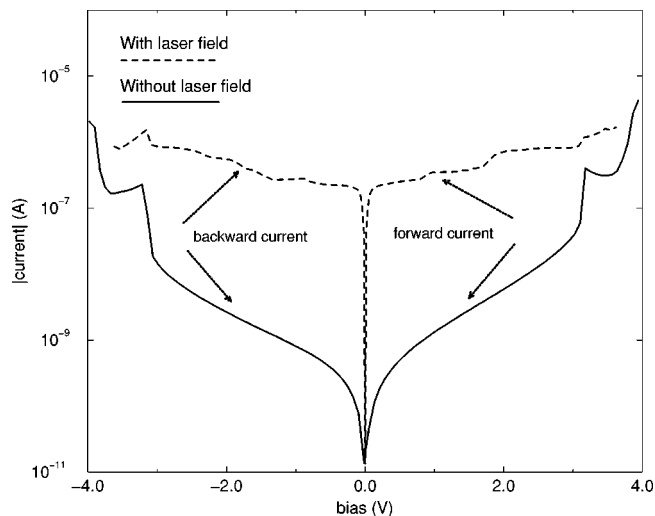


FIG. 9. I - V characteristic for the molecular wire system in the symmetric, break-junction geometry: the curve without the applied laser field is represented by the solid line, and the curve for the field-driven system is shown by the dashed line. The following field parameters apply: $\omega = 1.9$ eV and laser field strength $\mathcal{E}_0 = 2 \times 10^7$ V/cm.

B. STM (asymmetric) configuration

Here we consider an asymmetric (STM) system in which the left electrode-chemisorbed molecule distance is 1.9 \AA and the STM tip-molecule distance is 5 \AA . Again we choose a laser frequency of 1.9 eV, which corresponds to one half the HOMO-LUMO energy gap. Furthermore, we again fix the laser field amplitude at the value $\mathcal{E}_0 = 2 \times 10^7$ V/cm.

In Fig. 10 we show the forward (left to right) and backward (right to left) currents as a function of applied dc bias. Their difference (forward minus backward) gives the net left to right current through the wire. Notice that due to the asymmetric geometry of the STM configuration, the symme-

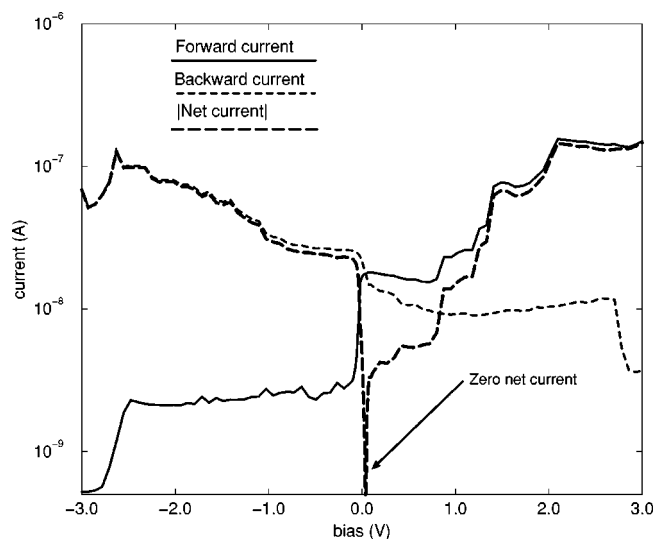


FIG. 10. Laser-assisted current through a xylyl-dithiol wire in the (asymmetric) STM configuration. As a function of applied dc voltage, forward current is shown via the solid line, backward current via the short-dashed line, and the absolute value of the net current is shown via the long-dashed line. The following field parameters apply: $\omega = 1.9$ eV and laser field strength $\mathcal{E}_0 = 2 \times 10^7$ V/cm.

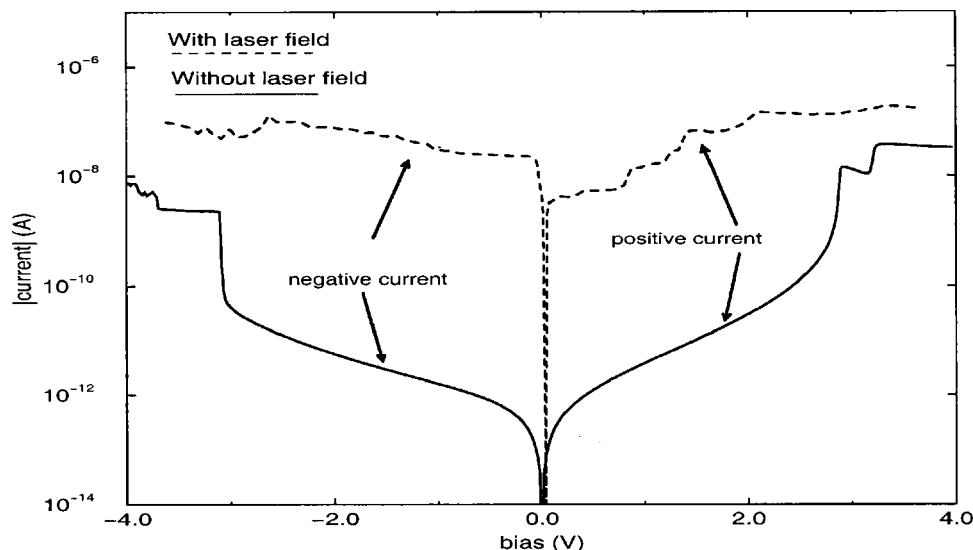


FIG. 11. I - V characteristic for the molecular wire system in the asymmetric, STM geometry: the result in the absence of the applied laser field is shown via the solid line; the corresponding result with the applied field is shown via the dashed line. The following field parameters apply: $\omega = 1.9$ eV and laser field strength $\mathcal{E}_0 = 2 \times 10^7$ V/cm.

try between forward and backward currents found in the break-junction case (*vide supra*) is broken. In particular, it is interesting to note that the forward and backward do *not* precisely cancel at zero dc voltage. In Fig. 11, we show via the dashed line the net current obtained under the input conditions just described as a function of applied dc bias. Again, this current represents the difference between forward current and backward current through the wire. The analogous result in the absence of the laser field is indicated via the solid line. We note that the value of current obtained for the “standard” wire (no laser field) is $\sim 10^{-11}$ A for a ~ 1 V dc bias, which is in order of magnitude agreement with experimental measurements on xylyl-dithiol systems using an STM apparatus.⁷ And, as in the break-junction case, it is clear that *large* enhancement of current flow (in fact, even larger than for the break-junction system studied in Sec. V A)

is obtained with a laser field of the amplitude and frequency noted above.

C. Estimation of laser field strengths needed for significant current enhancement

Here we tune the laser to resonance with the Fermi level to HOMO (and thus the Fermi level to LUMO) energy gap, i.e., we choose $\omega = 2.0$ eV. Then, for fixed applied voltage $V_{ap} = -0.4$ V, we study the dependence of the net electric current on laser field strength. Results are shown for both STM (asymmetric) and break-junction (symmetric) configurations in Fig. 12. In both cases we see that the backward current is much larger than the forward current, and hence accounts for almost the entire net current. For comparison, we also show the result obtained in the ICA approximation.

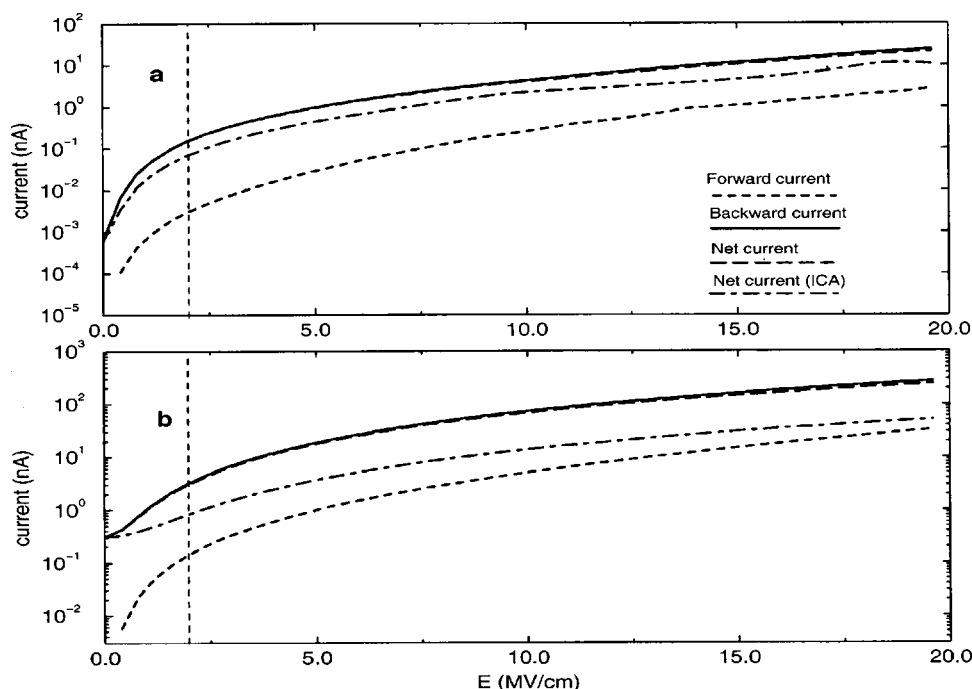


FIG. 12. Dependence of electron current on laser field strength for the STM case (top panel) and break-junction case (bottom panel). In each panel, the full Floquet Green’s function result for forward current is shown via the short-dashed line, backward current via the solid curve, and net current via the long-dashed curve. Net current computed within the ICA is shown via the dot-dashed line. The dashed vertical line highlights the large enhancements in net electric current obtained with a moderate laser field strength of 2×10^6 V/cm. Relevant parameters include: bias $V_{ap} = -0.4$ V and field frequency $\omega = 2$ eV.

The latter is seen to be reasonably good in the STM case and less so in the break junction case. (In the STM case, the large STM tip–molecule distance causes photon assist in the “tip to molecule” step of the electron tunneling transition to dominate intrabridge transitions; the latter require interreplica coupling and hence are not contained in the ICA.) It is clear that for both configurations substantial enhancement relative to the nondriven (laser-off) system is observed. For a moderate field strength of 2×10^6 V/cm (cf. Ref. 38) (located by the dashed vertical line), an enhancement of over 1 order of magnitude relative to the laser-free limit is obtained for the break-junction geometry, while an enhancement of more than 2 orders of magnitude is obtained for the STM configuration.

The essential effect of laser field illumination is to open up resonant photon-assisted conductance channels. The resultant resonant electron transfer processes depend only weakly on the number of sites through which the hopping takes place, i.e., the length of the molecular wire. In contrast, off-resonant electron transfer decreases *exponentially* with molecular wire length.¹⁸ Since the Fermi level of the metal contacts lies in the (multi-eV) gap between HOMO and LUMO orbitals of organic molecular wires like xylyl–dithiol and its multibenzene analogs, current through this class of molecular wire system is predicted, in the absence of laser illumination, to fall off dramatically (exponentially) with the length of the molecular wire (neglecting dissipative effects associated with coupling to a condensed phase environment³⁹). Thus we expect a larger field-induced enhancement factor for the electronic current as the molecular wire length increases.

VI. DISCUSSION AND CONCLUSION

In this paper we have applied the formalism developed in Part I¹⁴ to study electron transport through ac field-driven molecular wires in the particular case of xylyl–dithiol connected at either end to gold electrodes. The simplest possible level of description has been invoked, namely a one-electron tight-binding model for the electron dynamics. Dissipative coupling to an environment (for example, vibrations in the bridge molecule, phonons in the metal electrodes, and dipolar forces in a liquid solvent) has been neglected. Electron correlation effects, which would require a level of electronic structure theory considerably beyond the tight-binding model, are also ignored. Indeed, even if explicit electron–electron are ignored, the fermionic nature of the multielectron system involved here has only been treated crudely (via a one-electron model in which certain transitions are blocked based on the expected prior occupancy of the final states accessed by these transitions). Despite the success of this approach in understanding electron transport through nondriven molecular wires,^{7,16,17} a more rigorous treatment of Fermi statistics would be of interest in the field-driven case, which is further complicated by photon-assisted transitions. A related issue, unaddressed here, is the importance of hole current in the overall charge carrier transport process.

We showed in Part I that a molecular wire coupled to a monochromatic ac driving field such as results under laser illumination can be mapped, using Floquet theory, to an

equivalent ac field-free (“ordinary”) molecular wire system that corresponds to an augmented (formally infinite) electronic state space and appropriately renormalized interstate couplings. With this mapping, standard GF methods, applicable in the field-off case, can be utilized to compute the electron dynamics in the field-driven system. If a sufficiently large number of Floquet replica states are included in the calculation, a numerically exact solution of the field-driven dynamics can be obtained. We also presented in Part I an approximation scheme, the ICA, which simplifies the analysis of the Floquet Hamiltonian by neglecting certain inter-Floquet state couplings.

In the present paper this methodology was used to compute the net electric current through a xylyl–dithiol molecular bridge attached at either end to gold electrodes. Two geometric configurations were considered. One was symmetric with respect to the placement of electrodes on either side of the xylyl–dithiol molecule. A small electrode–molecule distance of 1.9 Å was employed in order to represent chemisorption of the sulfur atom from the xylyl–dithiol with gold atom(s) of the adjacent metal electrode. This was termed the “break-junction” configuration. A second configuration considered one of the gold electrodes to be significantly farther (5 Å) from the adjacent sulfur atom of the molecule. This asymmetric configuration was chosen to model an STM experiment in which the STM tip is at this distance from the molecule; hence it was termed the “STM” configuration. The geometric differences between these two configurations generate different electron–laser coupling, and hence lead to different induced currents when the same external fields are applied.

The parameters entering into the tight-binding model for this system were taken largely from EH level electronic structure calculations. While these are crude, they have provided useful qualitative estimations in previous studies on similar systems.⁷ Of course, improved electronic structure calculations would provide a valuable refinement of the overall theoretical treatment of electron transport through molecular wires, with or without laser driving.

The Fermi level of the electrodes (in the absence of applied dc voltage) lies near the middle of the HOMO–LUMO gap in xylyl–dithiol. This gap is almost 4 eV. In the absence of laser driving, and for modest applied dc bias, the tunneling electrons have energies approximately equal to the Fermi energy. Thus, tunneling is nonresonant and hence very inefficient, and the electron current is very small in the absence of any applied laser field. It is therefore desirable to illuminate the molecular wire/electrode system with light of a frequency which brings occupied electrode states into resonance with particular bridge molecular orbital energies. This dramatically increases the tunneling rate. Of course, one has to check that the final energy state of the *R* reservoir thus accessed is unoccupied and to balance (subtract) forward and backward currents. However, we showed in several examples that it is possible to do this in such a manner as to obtain a dramatically enhanced overall electric current through the wire, relative to the field-off analog.

Some testing of the accuracy of the ICA approximation in the context of the xylyl–dithiol molecular wire problem

was carried out. The ICA was seen to be qualitatively successful in most cases—successful enough to be used as a rough guide to the mechanism of current enhancement. However, for this particular molecule/model, the ICA was not successful at a quantitative level. In particular, photon absorption/emission *within* the bridge molecule itself, rather than during the hopping of the electron from electrode to bridge or vice versa, is significant under the experimental conditions considered here. Thus, the ability to converge the Floquet GF analysis by coupling together several bridge replicas proved important in obtaining an accurate evaluation of electron transport for this periodically time-driven system.

We cannot be absolutely sure that other effects, not considered in the present model, will not substantially modify these conclusions. Dissipation, the full constraints of fermion statistics, and electron correlation, mentioned above, are three such effects. We were also naive in our treatment of the influence of the laser field on the metal electrodes themselves. We assumed that this laser field did not excite direct electronic transitions between metal states. For real metals, it is well established that light *does* in general induce such transitions.⁴⁰ The effect of such processes on the overall tunneling current remains to be ascertained. Clearly, much work remains to be done on this complex but intriguing problem.

ACKNOWLEDGMENTS

We thank Professor Abraham Nitzan for several illuminating conversations on this topic. Work at the University of Pittsburgh was supported in part by National Science Foundation grant EEC 0085480. Many of the computations reported here were carried out at the University of Pittsburgh, Center for Molecular and Materials Science.

¹C. Joachim, *New J. Chem.* **15**, 223 (1991).

²See, for example, *Atomic and Molecular Wires*, edited by C. Joachim and S. Roth (Kluwer Academic, Dordrecht, 1997).

³G. Leatherman, E. N. Durantini, D. Gust, T. A. Moore, A. L. Moore, Z. Zhou, P. Rez, Y. Z. Liu, and S. M. Lindsay, *J. Phys. Chem. B* **103**, 4006 (1999).

⁴See, for example, *Molecular Electronics*, edited by M. A. Ratner and J. Jortner (Butterworth, London, 1997).

⁵L. A. Bumm, J. J. Arnold, M. T. Cygan, T. D. Dunbar, T. P. Burgin, L. Jones II, D. L. Allara, J. M. Tour, and P. S. Weiss, *Science* **271**, 1705 (1996).

⁶M. A. Reed, C. Zhou, C. J. Muller, T. P. Burgin, and J. M. Tour, *Science* **278**, 252 (1997).

⁷M. P. Samanta, W. Tian, S. Datta, J. I. Henderson, and C. P. Kubiak, *Phys. Rev. B* **53**, R7626 (1996); W. Tian, S. Datta, S. Hong, R. Reifenberger, J. I. Henderson, and C. P. Kubiak, *J. Chem. Phys.* **109**, 2874 (1998); S. Datta, W. Tian, S. Hong, R. Reifenberger, J. I. Henderson, and C. P. Kubiak, *Phys. Rev. Lett.* **79**, 2530 (1997).

⁸S. Datta, *Electronic Transport in Mesoscopic Systems* (Cambridge University Press, Cambridge, 1995).

⁹B. J. Keay, S. Zeuner, S. J. Allen, Jr., K. D. Maranowski, A. C. Gossard, U. Bhattacharya, and M. J. W. Rodwell, *Phys. Rev. Lett.* **75**, 4102 (1995).

¹⁰Y. Dakhnovskii and R. Coalson, *J. Chem. Phys.* **103**, 2908 (1995); D. G. Evans, R. D. Coalson, H. J. Kim, and Y. Dakhnovskii, *Phys. Rev. Lett.* **75**, 3649 (1995).

¹¹I. A. Goychuk, E. G. Petrov, and V. May, *Chem. Phys. Lett.* **353**, 428 (1996).

¹²Y. Dakhnovskii and H. Metiu, *Phys. Rev. B* **51**, 4193 (1995).

¹³M. J. Hagmann, *Appl. Phys. Lett.* **66**, 789 (1995); M. J. Hagmann, *J. Vac. Sci. Technol. B* **14**, 838 (1996).

¹⁴A. Tikhonov, R. D. Coalson, and Y. Dahnovsky, *J. Chem. Phys.* **116**, 10909 (2002).

¹⁵R. P. Andres, T. Bein, M. Dorogi, S. Feng, J. I. Henderson, C. P. Kubiak, W. Mahoney, R. G. Osifchin, and R. Reifenberger, *Science* **272**, 1323 (1996).

¹⁶M. Olson, Y. Mao, T. Windus, M. Kemp, M. Ratner, N. Leon, and V. Mujica, *J. Phys. Chem. B* **102**, 941 (1998).

¹⁷E. G. Emberly and G. Kirczenow, *Phys. Rev. B* **58**, 10911 (1998).

¹⁸V. Mujica, M. Kemp, and M. A. Ratner, *J. Chem. Phys.* **101**, 6849 (1994); **101**, 6856 (1994).

¹⁹C. Joachim and J. Vinuesa, *Europhys. Lett.* **33**, 635 (1996).

²⁰N. D. Lang, *Phys. Rev. B* **52**, 5335 (1995); M. Di Ventra, S. T. Pantelides, and N. D. Lang, *Phys. Rev. Lett.* **84**, 979 (2000).

²¹V. Mujica, A. Roitberg, and M. Ratner, *J. Chem. Phys.* **112**, 6834 (2000).

²²V. Mujica, M. Kemp, A. Roitberg, and M. Ratner, *J. Chem. Phys.* **104**, 7296 (1996).

²³In fact, if the site basis vectors $|I\rangle$ are associated with atomic orbitals of the bridge molecule, this condition is not strictly fulfilled. However, as will be shown in Sec. III C, it is straightforward to replace the atomic orbital basis with a slightly modified, strictly orthogonal site basis.

²⁴V. M. Akulin and N. V. Karlov, *Intense Resonant Interactions in Quantum Electronics* (Springer, Berlin, 1992).

²⁵S.-I. Chu, "Generalized Floquet theoretical approaches to intense-field multiphoton and nonlinear optical processes," in *Lasers, Molecules, and Methods*, edited by J. O. Hirschfelder, R. E. Wyatt, and Rob D. Coalson, Wiley Series on Advances in Chemical Physics, Vol. LXXIII (Wiley, New York, 1989).

²⁶To see that this expression is actually dimensionless, it is useful to restore \hbar : $\epsilon_0(\mu_\alpha - \mu_\beta)/\hbar\omega$.

²⁷S. Y. Hong and J. M. Song, *J. Chem. Phys.* **107**, 10607 (1997).

²⁸R. Hoffmann, *J. Chem. Phys.* **39**, 1397 (1963); J. P. Lowe, *Quantum Chemistry* (Academic, Boston, 1993).

²⁹M. J. Frisch, G. W. Trucks, H. B. Schlegel *et al.*, GAUSSIAN 94, Revision D.4, Gaussian, Inc., Pittsburgh PA, 1995.

³⁰I. V. Kurnikov and D. N. Beratan, *J. Chem. Phys.* **105**, 9561 (1996).

³¹M. J. Shephard, M. N. Paddon-Row, and K. D. Jordan, *Chem. Phys.* **176**, 289 (1993).

³²R. B. Ross, J. M. Powers, T. Atashroo, W. C. Ermler, L. A. LaJohn, and P. A. Christiansen, *J. Chem. Phys.* **93**, 6654 (1990).

³³D. A. Papaconstantopoulos, *Handbook of the Band Structure of Elemental Solids* (Plenum, New York, 1986).

³⁴R. Wiesendanger, *Scanning Probe Microscopy and Spectroscopy: Methods and Applications* (Cambridge University Press, Cambridge, UK, 1994).

³⁵S. Mukamel, *Principles of Nonlinear Spectroscopy* (Oxford University Press, Oxford, 1995), Chap. 2.

³⁶A. Tikhonov, R. D. Coalson, and Y. Dahnovsky (unpublished).

³⁷For this and subsequent calculations in which a nonzero value of the dc bias voltage is employed, we assume that the voltage drop is distributed linearly across the junction. Site energies of the bridge orbitals are shifted accordingly [cf. Eq. (1)] for each dc voltage considered.

³⁸Y. Kawata, C. Xu, and W. Denk, *J. Appl. Phys.* **85**, 1294 (1999).

³⁹W. B. Davis, M. R. Wasielewski, M. A. Ratner, V. Mujica, and A. Nitzan, *J. Phys. Chem. A* **101**, 6158 (1997).

⁴⁰A. Liebsch, *Electronic Excitations at Metal Surfaces* (Plenum, New York, 1997).